

Enhancing Solar Panels Efficiency: The Impact of Robotic Cleaning and Optimal Trajectory Tracking in the Presence of Disturbances Using Model Reference Adaptive Control

Yves Abessolo Mindzie^{a,*}, Joseph Kenfack^a, Brice Ekobo Akoa^b, Noé Paulin Frederic Ntoub^b, Blaise Njoya Fouedjou^a, Guy M. Toche Tchio^{a,c}, Joseph Voufo^a, Urbain Nzotcha^a

^aLaboratory of Energy, Water and Environment
National Advanced School of Engineering
University of Yaounde I
Ngoa-Ekélé, P.O. Box: 8390
Yaounde, Cameroon

^bLaboratory of Electrical and Telecommunication Engineering
National Advanced School of Engineering
University of Yaounde I
Ngoa-Ekélé, P.O. Box: 8390
Yaounde, Cameroon

^cLaboratory of Solar Energie
Regional Center of Excellence for Electricity Management
University of Lome
Boulevard Gnassingbé Eyadéma, Route de Tsévié, P.O Box: 1515
Lome, Togo

Abstract

The output power of photovoltaic systems (PV) can be significantly reduced by dust accumulation. Among various cleaning methods, robotic cleaning is currently the most popular choice because it minimizes human effort and reduces the risk of damaging PV cells. However cleaning robots can be impacted by various external disturbances, including wind, rain, lightning, snow, thunder, and vibrations. Additionally, sensor errors related to slip, position, velocity, acceleration, and varying electrical parameters can also affect their performance. Several methods have been proposed in the literature for tracking the robotic cleaning trajectory of PV systems. Nevertheless, most of these methods struggle in the presence of disturbances and often have prolonged convergence times. This paper aims to propose a Model Reference Adaptive Control system to maintain optimal performance and extend the lifespan of PV panels, minimize power losses, reduce convergence time, achieve optimal tracking of the desired cleaning trajectory amidst disturbances, and decrease the dependence on multiple sensors. In our study, we utilized the iRobot solar panel developed by Aravind et al., which has a power capacity of 250 W and weighs 250 kg. This iRobot can effectively clean approximately 930 solar panels of the Kyocera Solar KC 130 GT module, which measures 1.425 m in length and 0.652 m in width. The iRobot operates for 4 hours, covering an area of 864 m², and can clean a surface area of 0.06 m² in one second. We conducted simulations using the proposed MRAC algorithm in Matlab/Simulink software, comparing the results with those obtained from a Proportional Integral Derivative (PID) algorithm. The results demonstrate that the MRAC approach achieves a shorter convergence time and greater precision in following the desired cleaning trajectory of the robot, even in the presence of disturbances, compared to the PID algorithm.

Keywords: Robotic, Model Reference Adaptive Control, Cleaning, Trajectory, PV System

I. INTRODUCTION

A. Motivation

The energy demand has been steadily increasing in recent years due to factors such as population growth, industrialization, climate change, and the depletion of fossil fuels [1], [2], [3]. The production of energy is unable to meet this demand adequately, and the extraction of fossil fuels is declining [4]. Despite the

growing demand, other factors like the depletion of fossil fuels, rising oil prices, environmental issues associated with traditional energy sources such as global warming [5], the impact of carbon emissions from burning fossil fuels, and environmental pollution are driving us towards renewable energy [6]. Solar energy has been gaining more attention among all renewable energy sources due to its extensive functionality and the promise of lesser environmental impact. Additionally, solar energy is a primary and renewable energy source [7]. It is abundant, freely available, does not require transportation, and does not cause environmental pollution. PV technology offers several benefits, including high cleaning effectiveness, declining PV module costs, extended service lives, straightforward

* Corresponding Author.
Email: abessoloyves88@gmail.com

Received: June 19, 2024 ; Revised: November 10, 2024
Accepted: November 20, 2024 ; Published: December 31, 2024

installation, and affordable maintenance costs [8]. The most expensive and crucial component of a solar power system is its core: the solar panels. Their main function is to convert solar energy into electricity. Apart from the rapidly changing atmospheric conditions (temperature and irradiance), it is well-known that dust accumulation, bird droppings, and other harmful substances on the surface of PV panels significantly affect their performance negatively [9]. Among the various PV cleaning methods described in the literature, the automatic cleaning robot system is highly regarded due to its consideration of issues such as the need for human PV cleaning efforts, the complexity of the cleaning process, the low PV efficiency, and the time-consuming, labor-intensive, and expensive nature of PV cleaning costs [10].

B. Literature Review

Solar panels are exposed to various weather-related elements throughout the year, like dirt, accumulated dust, atmospheric pollution, and bird droppings. As a result, numerous methods for cleaning solar panels have been explored, some of which may improve their performance. In addition, experts concur that dust accumulation on solar panels contributes to a loss in energy output [11]. Increasing the power generation efficiency of solar photovoltaic panels by 1-2 percentage points will require significant research and development investment. The photoelectric effect of silicon photovoltaic panels can be greatly impacted by sun-blocking dust, resulting in a 35-40% reduction in power generation efficiency [12]. Dust accumulation and soiling reduce the transmittance of the glass cover, thereby decreasing the efficiency of PV panels [13]. Dust accumulation causes a decline in the power generation of panels by up to 15% per day by reducing incoming solar radiation [14]. In arid places with appropriate irradiance, dust accumulation is a critical issue, as widespread dust, sandstorms, and a lack of rain deposit dust on panel surfaces, impact the operation of PV panels [15]. The lifespan of the PV system is shortened in many circumstances because dust build-up on the surface of PV panels causes mismatch losses, which can result in hotspots that could harm the panels [16], [17]. Zhen et al [18] advise that routine cleaning of solar panels is crucial because, without it, the impact of dust will be significant. Numerous water-based and water-free approaches for cleaning the surface of panels can be used to mitigate the unwanted effect of soiling [19]. Satpathy et al [20] Suggest a method based on the electrostatic force for sand removal from the PV panel surface, which is particularly suitable for low-latitude desert regions. PV panel surfaces can now be cleaned automatically and without using water [5], [21]. The efficiency of solar photovoltaic panels would be less affected by airborne dust if they were covered in a super hydrophobic micro-shell Polydimethylsiloxane (PDMS) array [22]. When used for covering solar panels, this superhydrophobic material typically achieves 90% dust-proof efficiency after cleaning. To reduce the likelihood of dust accumulation, a line of superhydrophobic materials is based on the photocatalytic activity of TiO₂ compounds [23]. However, a major drawback of this

technology is that each solar panel must have these specific coatings sprayed on them, incurring additional costs, and their adhesion will deteriorate over time due to exposure to sunlight.

The wet cleaning method is more successful than the dry cleaning method in removing dust particles from surfaces [2]. The automated cleaning and 360° sun monitoring technology produces a 30% greater power output compared to flat photovoltaic panels. It highlights the peeling-off effect on self-cleaning surfaces. There are three negative consequences when the illumination intensity decreases due to light being blocked by dust layers on the panels: (1) formation of hotspots and dead cells if dust layer deposits partially cover the modules, (2) reduction in power output, and (3) decrease in overall efficiency. An overview of various water-free methods using robotic equipment for PV panel cleaning can be found in [24].

One potential approach for effectively cleaning PV panels is the use of autonomous robots [25][26]. Many people employ robots for cleaning tasks, and mobile robots are often preferred for cleaning solar panels due to their ability to cover large surfaces. To clean PV panels, it is essential to utilize cleaning robots that can navigate the tilted surface of the panels, which are inclined for optimal solar energy absorption [27]. Therefore, the robots must incorporate an adhesion mechanism to walk on the PV panel surface. In our business, we are specifically interested in self-cleaning, four-wheeled mobile robots that can be initiated manually or automatically. This is the underlying reason behind the discussion of a robot cleaning system [28], where the robot is controlled by an Arduino microcontroller. To ensure self-cleaning robots accurately follow their intended path during the cleaning process, a high degree of precision is required [29]. The desired trajectory, however, is not always fully achieved due to variable and uncertain parameters, the influence of certain parameters not considered during modeling, external disturbances such as changes in electrical parameters and equipment aging, and sensor measurement errors including slip, velocity, distance, acceleration, etc. Hence, there is a need to model and manage this system of self-cleaning robot.

In Cameroon, where the climate is often dry and dusty, regular cleaning of the panels is essential to maintain their performance. Robotic cleaning of solar panels is emerging as an innovative solution to maximize energy production while reducing maintenance costs. Robotic cleaners can enhance the efficiency of solar panels by ensuring regular and thorough cleaning, allowing for better absorption of sunlight. Robotic cleaning of solar panels represents a significant opportunity to improve energy efficiency in Cameroon. By overcoming the associated challenges, this technology can play a key role in the transition to sustainable and efficient solar energy [29], [30].

In Cameroon, the frequency with which a cleaner robot cleans solar panels can vary based on several factors, including :

1. Location: Areas with more dust, pollen, or pollution may require more frequent cleaning.

2. Weather Conditions: Rain can help clean panels naturally, reducing the need for manual cleaning afterward.
3. Panel Orientation: Panels facing certain directions may accumulate dirt more quickly.
4. Season: Different seasons may affect the rate of dirt accumulation due to factors like falling leaves or winter snow.

Typically, cleaner robots might operate anywhere. In Cameroon, it could be from once a week to once a month, depending on these factors. It's essential to monitor the panels and adjust the cleaning schedule accordingly to maintain optimal efficiency [31].

The four-wheeled robot is designed in an inverted pendulum style and is mounted on a cart with four wheels. Operating on the same principles as an inverted pendulum, this unstable and non-linear robotic system has become a testing ground for various control strategies [30][31]. The control of the four-wheeled robot's behavior, characterized by its nonlinear and unstable nature, has gained popularity in the scientific community. Many authors have researched these robots to develop an ideal mathematical model and define its structure.

Numerous control algorithms have been proposed in the literature for the control of cleaning robots and their intended tracking of cleaning trajectory [32]. One commonly used algorithm is the traditional Proportional Integral Derivative (PID) control, which is popular in the industrial sector due to its low manufacturing cost and simplicity [33]. However, designing robots that operate in unstructured environments with uncertainties presents a major challenge [22]. These uncertainties arise from factors such as inaccurate sensors, unpredictable environmental variables, and complex dynamics [34].

To address these challenges, an adaptive control strategy has been developed. Additionally, several adaptation laws have been created to calculate the controller parameters and evaluate the local or global stability of the controlled system [35]. These laws include Model Predictive Control (MPC) [36], Fuzzy Logic Control (FLC), Kalman Filter algorithm (KF), Sliding Mode Control (SMC), and Artificial Potential Field (APF). While these adaptive laws are robust against disturbances, they often suffer from implementation complexity [37], [38]. The system response may oscillate, leading to reduced stability, especially when the mechanical design is inflexible and the control mechanism is unable to handle uncertainty.

To enhance the control of mobile robots during cleaning processes, various intelligent algorithms have been proposed in the literature. For instance, in [39], two alternative techniques, namely Linear Quadratic Gaussian (LQG) and Model Predictive Control (MPC), were compared and applied to a two-wheeled robot. The results demonstrated that LQG control outperforms the other technique. However traditional feedback controllers have limitations, as stated in several control methods, due to the incomplete achievement of accurate mobile robot movement. This is primarily attributed to dynamic uncertainties resulting from environmental changes [40].

Several optimization algorithms have been introduced in the literature, including the Optimizer Overhead algorithm (OOA), Genetic Algorithm (GA), Neural Networks algorithm (NN), Evolutionary Optimization Algorithm (EOA), Algorithm Effort (AE), Intelligent Service Control (ISC) algorithm [41], Machine Learning (ML) algorithm [42], Differential Evolution (DE), Harmony Search (HS), Bat Algorithm (BA), Invasive Weed Optimization (IWO), Ant Colony Optimization (ACO), Bacterial Foraging Optimization (BFO), Probabilistic Cell Decomposition (PCD), Bug Algorithm (BA), the Vector Field Histogram (VFH), and Virtual Force Field (VFF) algorithm [43].

Furthermore, adaptive algorithms, such as Adaptive Sliding Mode Control (ASMC) and Non-Linear Model Predictive Controller (NMPC), have also been proposed in the literature [44]. While these intelligent algorithms can adapt to disturbances, they suffer from long response times, high implementation complexity, and increased energy consumption for the cleaning robot.

C. Contribution

We have observed in the literature that most of the works use the PID algorithm for the trajectory tracking control of cleaning solar panels by mobile robotic cleaners. This is the case, for example, of the work of Aravind et al., which we have taken as an example in this paper. However, the literature also presents the PID algorithm as a control that is very sensitive to disturbances. Solar panel cleaning robots can be confronted with disturbances such as lightning, thunder, vibrations, and sensor errors (such as slippage, position, and acceleration errors). By using the PID control for the trajectory tracking of solar panel cleaning by mobile robots :

1. Firstly, there is small energy losses due to the response time to the cleaner robot to operate the cleaning process of solar panels bot without or in, face of disturbances.
2. Secondly, in case of disturbances these solar panels will be poorly cleaned. The poor cleaning of solar panels will lead to hot spots on the solar panels, will not allow the solar rays to reach the entire surface of the solar panels, and will lead to the modification of the electrical parameters, power losses, and a decrease in the efficiency of the PV systems [15]. To avoid these power losses and a decrease in the efficiency of the PV systems due to poor cleaning, we have proposed the MRAC approach to reduce the response time of any robotic cleaner solar panels and for optimal tracking of the desired cleaning trajectory of solar panels by mobile robots. This MRAC approach will be able to follow the desired cleaning trajectory of the solar panels by any mobile solar panel cleaning robot, taking into account the disturbances that this mobile solar panel cleaning robot may undergo during its cleaning process with a small convergence time.

D. Organization

The remainder of the paper is organized as follows: The self-cleaning system is described in the second

section, the proposed algorithm is presented in the third section, and the self-cleaning robot is simulated in the fourth section, titled "Simulation Results and Discussion," where discussions are also provided. The fifth section will conclude the research work discussed in the paper and present the conclusions.

II. MATERIALS AND METHOD

A. Materials

1) Presentation of the self-cleaning solar panels

Here, a robot vacuum cleaner is proposed for self-cleaning solar panels [45], [4]. The robot used here for our work is a cleaner panels robot called iRobot, developed by Aravind et al., and represented in Figure 2, it has a power capacity of 250 W and weighs 250 kg. This iRobot can effectively clean approximately 930 solar panels for a solar panel that measures 1.425 m in length and 0.652 m in width. This iRobot can operate for up to 4 hours, covering an area of 864 m², and it is capable of cleaning a surface area of 0.06 m² in 1 second [4]. It operates under a working voltage of 12 V DC, at a frequency of 50 Hz, and uses a 12.6 V DC battery, 100 AH, capable of supporting a current of 20 A and taking approximately 5 hours to charge.

The robot is self-sufficient because it can be powered by the PV panel array and does not need any additional external power sources. As shown in Figure 1, a predetermined path covers the entire area of the solar panels. The robot moves back and forth along this path. Ultrasonic sensors and accelerometers provide feedback by avoiding cliffs and detecting edges.

The software components are such that the robot traverses the path as shown in Figure 1. This predefined path ensures that the total expanse of the solar panels is effectively covered. To stay on the defined path, the output signals from the accelerometers are processed by the MSP430G2553 Microcontroller and compared with a pre-defined set of values.

The PID control technique is implemented by adding the calculated error to the timer's capture/compare register value which alters the Pulse Width Modulation (PWM) signal given as input to the motor driver. The hardware components of the iRobot are such that the motors used are 12V, 5 kg-cm torque, 60 PM side-shaft Geared DC motors. The gears are attached to a 12V, 300 RPM side-shaft DC geared motor. The vacuum motor is a 20000 RPM Johnson motor. The LM3914 dot/bar display driver is used to

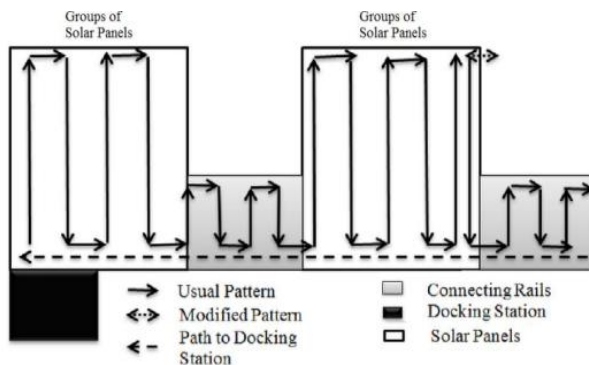


Figure 1. Path-Plan

indicate the voltage level based on battery voltage. The TPIC0298 motor driver is used for controlling the motors as necessary. The microcontroller is powered from 3.3V supplies obtained via Buckconverter (LM2675-3.3). The iRobot solar cleaner panels has the following analog circuits : Master control Board, Buck converter, Battery Level Indicator and Motor driver. In the DC charging circuit, a variable voltage regulator LM317 is used to set the required maximum charge voltage at 12,6 V (see Figure 2) [4].

The proposed cleaning system is implemented by developing two subsystems, as follows [45]:

- Docking Station: The docking station is set up at the beginning of the solar panels. It has a base with two aluminum strips mounted, serving as the positive and negative terminals.
- Robotic Vacuum Cleaner: Dust on solar panels accumulates into a sticky film that is challenging to remove with a portable vacuum cleaner. As a result, a two-stage cleaning procedure is implemented. In Stage 1, a rolling brush is attached to the robot in a manner that agitates the dust and propels it towards the vacuum cleaner [4]. In Stage 2, the vacuum motor generates sufficient suction to collect the dust scattered around the solar panel. The presence of a sticky dust layer on a smooth, inclined surface exacerbates slippery conditions. To address this, gripper wheels are utilized to enhance traction while moving across the solar panels. The MSP430G2553 microcontroller serves as the primary control component for steering the robot. The design of the robot focuses on minimizing the overall weight to improve efficiency and prolong battery life. Figure 2 illustrates the hardware setup representation of the robot [4].

2) Mathematical model of DC-DC four-wheel motors of the robotic cleaner of solar panels

A model of the DC-DC motor, consisting of the set of equations presented here, can be regarded as a nonlinear dynamic system. The electrical equivalent circuit of a DC-DC motor is depicted in Figure 3. Let us consider the table 1 of the parameters of DC-DC wheel

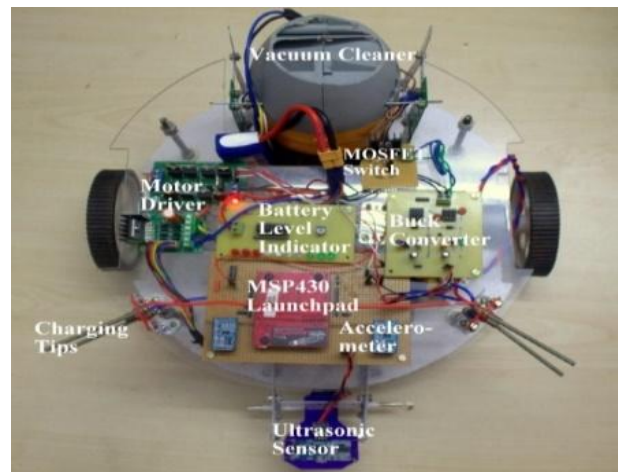


Figure 2. Robotic cleaner of solar panels [4]

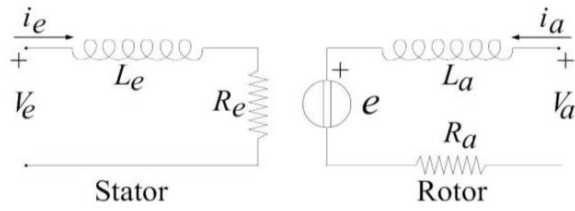


Figure 3. Electrical equivalent scheme of a DC-DC motor

 TABLE 1
 DC-DC WHEELS MOTOR CONTROL PARAMETERS [4]

Parameters	Units
Stator resistance ($R_e = r$)	Ω
Inductor current ($i_e = i$)	A
Rotor current (I)	A
Magnetic flux (Φ)	Wb
Motor friction ($B = B_m$)	N.m.s
Position (θ)	m or rad
Stator voltage ($V_e = V_b = u$)	V
Rotor voltage ($U = V_a = e$)	V
Rotor resistance ($R_a = R$)	Ω
Moment of motor inertia ($J = J_m$)	Kg.m ²
Motor torque ($K = K_b = K_a$)	N.m
Electric inductance ($L = L_a = L_e$)	H
Angular velocity (Ω)	Rad/s
Electromagnetic torque (C_{em})	N.m
Resistive torque (C_r)	N.m
Coefficient of friction ($C_f = f$)	N.m
Electromagnetic power (P_{em})	W

motor control. The electric equations for the rotor and stator take into account the equality of the stator and rotor inductors ($L_a = L_e = L$). We have the following equation at the rotor (see equations (1) and (2) [44]):

$$U = RI + L \frac{di}{dt} + E = RI + L \frac{di}{dt} + K \cdot \Omega \cdot \Phi \quad (1)$$

at the stator ($i = i_e$), we have equation (2):

$$u = ri + L \frac{di}{dt} \quad (2)$$

The mechanical equations for the rotor and stator are given by equation (3) [44]:

$$J \frac{d\Omega}{dt} = C_{em} - C_r - C_f; P_{em} = C_{em} \cdot \Omega \quad (3)$$

Applying the Laplace transform, equations (1) and (3) can be expressed in terms of the Laplace variable s (equations (4) and (5) [44]):

$$(Ls + R)I(s) = U(s) - Ks\theta(s) \quad (4)$$

$$s(Js + B)\theta(s) = KI(s) \quad (5)$$

Taking Laplace transform obtained in equations (4) and (5) of equation of the rotor and mechanical equations, the transfer function of the DC motor can be obtained as shown in equation (6) [44]:

$$Y(s) = \frac{\Omega(s)}{U(s)} = \frac{\frac{K}{JL}}{\left[s^2 + \frac{(JR+BL)}{JL}s + \frac{(BR+K^2)}{JL} \right]} \quad (6)$$

The transfer function (shown in equation (6)) presents that the rotational speed Ω ($\Omega = \omega$) is

considered the output, and the armature voltage is considered the input, U_a ($U_a = U$). Then, we converted it into a block diagram, as shown in Figure 4.

B. Method

1) Proposed control

The model reference adaptive control (MRAC) is the proposed algorithm, it is based the use a reference model to specify the desired system performance. It was developed to address servo issues [35], [46], [47]. The control algorithm adjusts the system parameters at each step to achieve asymptotic convergence between the system output and the reference model [48]. The fundamental idea behind the reference model adaptive control is to modify the controller's settings in response to the difference between the system and the reference model. Figure 5 illustrates the structure of the MRAC algorithm.

2) Mathematical model of the reference model

The adaptive control system's optimal response to an external command is determined by a reference model [48]. This model represents the desired behavior that the adaptation mechanism should aim for when adjusting the parameters. Essentially, it provides a general overview of the expected system response to a specific input and models a subset of that behavior [48].

The reference model is also represented in the second-order transfer function of the DC-DC motor (shown in equation (6) [48], where C_m is a positive gain and A_m and B_m are selected to achieve a critically damped step response. The desired natural frequency (ω_n) and damping ratio (δ) are known and used in this representation (see equation (7)) [48]:

$$Y_m(s) = \frac{C_m}{s^2 + A_m s + B_m} = \frac{\omega_n^2}{s^2 + 2\delta\omega_n s + \omega_n^2} \quad (7)$$

3) Controller structure

The structure of the controller allows us to obtain the objective control function is depicted in Figure 6 [48]. According to the controller structure in Figure 8, we have the expression of the control (see equation (8)) [49]:

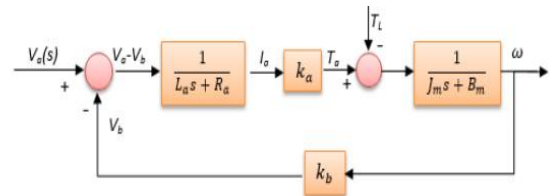


Figure 4. Block diagram of a DC motor of wheel control of vacuum cleaner robot

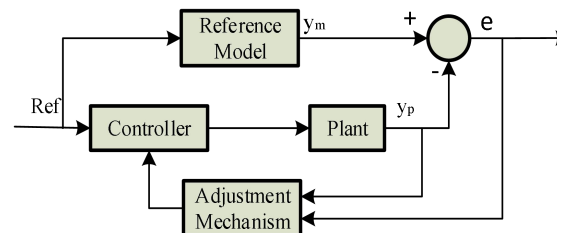


Figure 5. Structure of the proposed MRAC algorithm

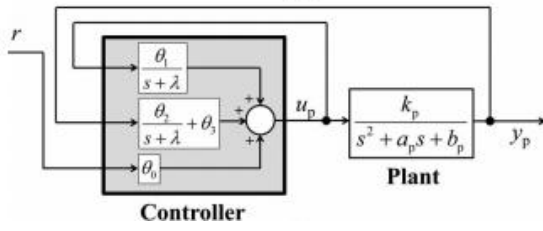


Figure 6. Controller structure.

$$u_p = u_0 r + \theta_1 \frac{1}{s+\lambda} u_p + \theta_2 \frac{1}{s+\lambda} y_p + \theta_3 = \theta_0 r + \theta_1 \omega_1 + \theta_2 \omega_2 + \theta_3 y_p = \theta^T \omega \quad (8)$$

where the vector parameter of the controller is represented by equation (9) [49]:

$$\theta = [\theta_0, \theta_1, \theta_2, \theta_3]^T \quad (9)$$

And we have equation (10) [49]:

$$\omega = [\theta, \omega_1, \omega_2, y_p]^T \quad (10)$$

with $\omega_1 = \frac{1}{s+\lambda} u_p$, $\omega_2 = \frac{1}{s+\lambda} y_p$, and $\frac{1}{s+\lambda}$ the stable filter (see equation (11)) [49]:

$$\begin{cases} \dot{\omega}_1 = -\lambda \omega_1 + u_p \\ \dot{\omega}_2 = -\lambda \omega_2 + y_p \end{cases} \quad (11)$$

where :

- Ω is the angular velocity (rad/s);
- r is the designed position;
- u_p is the control signal;
- θ is the position (m or rad);
- y_m is the output signal of the reference model;
- y_p is the output signal of the dc motor (plant);
- λ is the adaptation gain;
- a, b, k_p are constants;
- e is an error signal;
- $\Phi, \theta^*, \bar{\theta}, \bar{e}$ are a control parameters.

By observing the structure of the controller and the principle of the MRAC algorithm, we will have as condition the relations: $\frac{y_p(s)}{r(s)} = \frac{y_m(s)}{r(s)}$ with the new controller setting is represented in equation (12) [49]:

$$\theta^* = [\theta_0^*, \theta_1^*, \theta_2^*, \theta_3^*] \quad (12)$$

with $\theta_0^* = \frac{k_m}{k_p}$, $\theta_1^* = a_p - a_m$, $\theta_2^* = \frac{(a_p - a_m)(-\lambda^2 - \lambda a_p - b_b)}{k_p}$ and $\theta_3^* = \frac{(b_p - b_m) + (a_p - a_m)(\lambda - a_p)}{k_p}$.

4) Mathematical model of the solar panels cleaner robot

The state equations models of the wheels motor of solar panels cleaner robot is explained in this section. According to equations (4) and (5), we then have equation (13) [50]:

$$\begin{bmatrix} \dot{X}_1 \\ \dot{X}_2 \\ \dot{X}_3 \end{bmatrix} = \begin{bmatrix} -R & -K & 0 \\ L & L & 0 \\ K & -f & 0 \\ 0 & J & 1 \end{bmatrix} \begin{bmatrix} X_1 \\ X_2 \\ X_3 \end{bmatrix} + \begin{bmatrix} 1 \\ L \\ 0 \end{bmatrix} U + \begin{bmatrix} 0 \\ -1 \\ J \\ 0 \end{bmatrix} G \quad (13)$$

Let us pose equation (14) [49] :

$$\begin{cases} \dot{X}_1 = I \\ \dot{X}_2 = \Omega \\ \dot{X}_3 = \Phi \end{cases} \text{ where } \begin{cases} \dot{X}_1 = I \\ \dot{X}_2 = \Omega \\ \dot{X}_3 = \Phi \end{cases} \quad (14)$$

Considering $Cr = 0$, equation (13) becomes equation (15) [49]:

$$\begin{bmatrix} \dot{X}_1 \\ \dot{X}_2 \\ \dot{X}_3 \end{bmatrix} = \begin{bmatrix} -R & -K & 0 \\ L & L & 0 \\ K & -f & 0 \\ 0 & J & 1 \end{bmatrix} \begin{bmatrix} X_1 \\ X_2 \\ X_3 \end{bmatrix} + \begin{bmatrix} 1 \\ L \\ 0 \end{bmatrix} U \quad (15)$$

Equation (15) then become equation (16) for representing the state model of the cleaner driver motor[49]. Let's consider the set A_p, B_p, C_p and the realization to minimize $G_p(s)$:

$$\begin{cases} \dot{x}_p = A_p x_p + B_p u_p \\ y_p = C_p x_p \end{cases} \quad (16)$$

where x_p is a vector of dimension 3 (3-D). Considering equations (15) and (16), the closed loop of the system and the controller has the state equation as shown in equation (17) [49] :

$$\begin{cases} \dot{x}_{pe} = A_{pe} x_{pe} + B_{pe} \theta_0^* r \\ y_p = C_{pe} x_{pe} \end{cases} \quad (17)$$

where x_{pe} is an extended state vector defined by:

$$x_{pe} = [x_p^T, \omega_1, \omega_2]^T \quad (18)$$

The matrices A_{pe}, B_{pe} , and C_{pe} are defined by equations (18), (19), and (20) [49]:

$$A_{pe} = \begin{bmatrix} A_p + \theta_3^* B_p C_p & \theta_1^* B_p & \theta_2^* B_p \\ \theta_3^* C_p & -\lambda + \theta_1 & \theta_2^* \\ C_p & 0 & -\lambda \end{bmatrix} \quad (19)$$

$$B_{pe} = \begin{bmatrix} B_p \\ 1 \\ 0 \end{bmatrix}; C_{pe} = [C_p \quad 0 \quad 0] \quad (20)$$

where, $u_p = \theta^{*T} \omega$. Then, equation (17) becomes (see equation (21)) [49]:

$$\begin{cases} \dot{x}_{pe} = A_{pe} x_{pe} + B_{pe} \theta_0^* r \\ y_p = C_{pe} x_{pe} \end{cases} \quad (21)$$

Then, the set $\{A_{pe}, B_{pe}, \theta_0^*, C_{pe}\}$ allows us to obtain the reference model which will have as equation of state defined in equation (22) [49]:

$$\begin{cases} \dot{x}_{me} = A_{pe}x_{me} + B_{pe}\theta_0^*r \\ y_m = C_{pe}x_{me} \end{cases} \quad (22)$$

where x_{me} is a four-dimensional state vector. It can be verified that A_{pe} is asymptotically stable.

5) Stability study of the solar panels cleaner robot

a) Equation error

The equation of state for the error, the parameters of the error controller, and the error tracker are determined by differentiating the equations of state of the system to be controlled and the reference model as shown in equation (23) [49]:

$$\begin{cases} \dot{e} = A_{pe} + B_{pe}(u_p - \theta^{*T}\omega) \\ e_0 = C_{pe}e \end{cases} \quad (23)$$

where $e, e_0, \tilde{\theta}$ represent: the state error, the error tracker and the error controller parameter, respectively according to equation (24) [49]:

$$\begin{cases} e = x_{pe} - x_{me} \\ e_0 = y_p - y_m \\ \tilde{\theta} = \theta - \theta^* \end{cases} \quad (24)$$

The input-output matching law of the transfer function equation of the error state vector must be strictly positive to satisfy the Lyapunov criterion [49]. However, the transfer function (shown in equation (21)) does not strictly satisfy this requirement due to the following reasons (see equation (25)) [49]:

$$C_{pe}(SI_i - A_{pe})^{-1}B_{pe} = \frac{G_m(s)}{\theta_0^*} \quad (25)$$

From equation (25) and the relative degree of $G_m(s)$ is two, which implies that $\frac{G_m(s)}{\theta_0^*}$ is not defined as strictly positive (with I_i the identity matrix). To overcome this difficulty, we use the identity: $(s+g)(s+g)^{-1} = 1$, for all $g > 0$ and equation (23) will be written as equation (26) [49]:

$$\begin{cases} \dot{e} = A_{pe} + B_{pe}(s+g)(u_g - \theta^{*T}\omega) \\ \dot{e} = A_{pe} + B_{pe}(s+g)\tilde{\theta}^T\phi \end{cases} \quad (26)$$

where the term $s+g$ allows the degree of the numerator to grow to make the transfer function equals to one. However, the controller can be expressed as equation (27) [49]:

$$\begin{cases} u_g = (s+g)u_g \\ u_g = \theta^{*T}\phi + \theta^T\omega \\ u_g = \dot{\theta}^T\phi + \theta^T(\phi + g) \\ u_g = \dot{\theta}^T\phi + \theta^T\omega \\ \bar{e} = e - B_{pe}\tilde{\theta}^T\phi \end{cases} \quad (27)$$

Its derivative gives equation (28) [49]:

$$\begin{cases} \dot{\bar{e}} = A_{pe}\bar{e} + (A_{pe}B_{pe} + gB_{pe})\tilde{\theta}^T\phi \\ e_0 = C_{pe}\bar{e} + C_{pe}eB_{pe}\tilde{\theta}^T\phi \end{cases} \quad (28)$$

Let $B_1 = A_{pe}B_{pe} + gB_{pe}$ and $C_{pe}B_{pe} = 0$ because the degree of the reference model is two, i.e., the largest coefficient in the numerator: $C_{pe}(SI_iA_{pe})^{-1}B_{pe} = 0$. Therefore we will have equation (29) [49]:

$$\begin{cases} \dot{\bar{e}} = A_{pe}\bar{e} + B_1\tilde{\theta}^T\phi \\ e_0 = C_{pe}\bar{e} \end{cases} \quad (29)$$

For the new state error (equation (29)), its transfer function from $\tilde{\theta}^T\phi$ to e_0 in equation (23) makes the set $\{A_{pe}, B_{pe}, C_{pe}\}$ has the transfer function shown in equation (30) [49]:

$$(s+g)\frac{G_m}{\theta_0^*} = \frac{Km}{\theta_0^*} \frac{(s+g)}{s^2+a_ms+b_m} \quad (30)$$

The positive constant g is chosen such that $g < a_m$. It can be shown that equation (29) is strictly positive definite for any g such that $0 < g < a_m$.

b) Derivation of the adaptation law

By deriving the adaptation law, we construct a Lyapunov function having two state vectors such as the controller parameter error θ and the state error (see equation (31)) [49]:

$$V(\tilde{\theta}, \bar{e}) = \frac{\bar{e}^T P \bar{e}}{2} + \frac{\tilde{\theta}^T \Gamma^{-1} \tilde{\theta}}{2} \quad (31)$$

where P is a positive definite symmetric matrix established by the Meyer-Kalman-Yakubovich (MKY) Lemma, and Γ is an arbitrarily positive definite symmetric matrix. According to the MKY Lemma, there exists a symmetric positive definite matrix P , a vector q , and a scalar, since A_{pe} is stable and " A_{pe}, B_{pe} , and C_{pe} " are specified as strictly positive in equation (31). For $V > 0$, we get equation (32) [49]:

$$\begin{cases} PA_{pe} + A_{pe}^T P = -qq^T - V \\ PB_1 = C_{pe}^T \end{cases} \quad (32)$$

For any given symmetric positive definite matrix L , matrix P in equation (29) satisfies equation (32). The time-derivative of the Lyapunov function (equation (28)) along the solution of equation (31) can be calculated as in equation (33) [49]:

$$\dot{V} = (\tilde{\theta}, \bar{e}) = -\frac{1}{2}\bar{e}^T qq^T \bar{e} - \frac{V}{2}\bar{e}^T L \bar{e} + \bar{e}^T PB_1 \tilde{\theta}^T \phi + \tilde{\theta}^T \Gamma^{-1} \dot{\tilde{\theta}} \quad (33)$$

Since, we can choose equation (34) [49]:

$$\dot{\tilde{\theta}} = -\tilde{\theta} - \Gamma e_0 \phi \quad (34)$$

thus we have equation (35) [49]:

$$\dot{V} = (\tilde{\theta}, \tilde{e}) = -\frac{1}{2}\tilde{e}^T q q^T \tilde{e} - \frac{V}{2}\tilde{e}^T L \tilde{e} \leq 0 \quad (35)$$

Condition in equation (34) must always be met for the adaptation law as shown in equation (35), which ensures that the tracking error and control parameter error are stable and constrained. The general MRAC rules can be deduced from the aforementioned derivations as shown in equation (36) [48], [49]:

$$\begin{cases} \dot{\omega}_1 = -\lambda\omega_1 + u_p \\ \dot{\omega}_2 = -\lambda\omega_2 + y_p \\ \dot{\phi} = -\dot{g}\phi + \omega \\ u_p = \theta^T + \dot{\theta}^T \phi = \theta^T \omega - \phi^T \Gamma e_0 \phi \\ \dot{\theta} = -\Gamma e_0 \phi \end{cases} \quad (36)$$

6) *Simulink block diagram of MRAC control of wheels motors of cleaner robot*

To accurately trace the cleaning trajectory as specified by the vacuum cleaner robot, Figure 7 illustrates the Simulink diagram showcasing the control of the wheel motors through the suggested MRAC control algorithm.

III. RESULTS AND DISCUSSION

A. Results

Here, the self-cleaning system under study is a vacuum cleaner robot design described in the literature. It operates at an operating voltage of 12V DC and utilizes a 12.6V DC battery to supply power while removing collected dust and grime from solar panels. Step and square wave references will be employed for control purposes. The simulation results will be obtained using Matlab/Simulink software.

1) *Electrical parameters and model with no-load of cleaning stepper motor of wheels control*

The electrical specifications of the DC motors that we will use to drive our vacuum cleaner robot, both for powering the rollers and for the motion of the wheels, are shown in Table 2. These specifications were provided by the works of Aravind et al [4] to assist us in evaluating the performance of the controller.

According to the values of parameters of the dc wheels control motor in Table 2 and (32) of its transfer

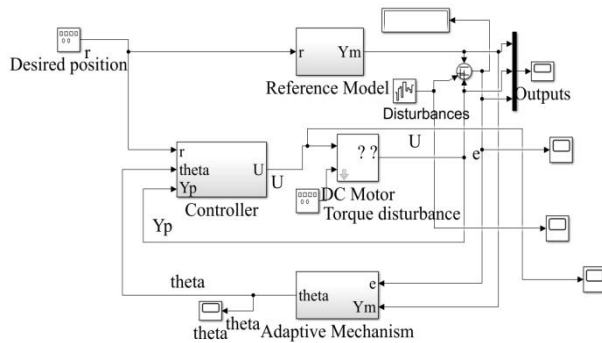


Figure 7. Simulink block diagram of the wheel motor control for a cleaner robot using the MRAC control algorithm

TABLE 2
ELECTRICAL PARAMETERS OF CLEANING STEPPER MOTOR [4]

Parameters	Values	Units
Operating voltage (U) (DC)	12	V
Speed (Ω)	20000	RPM
Motor torque (K)	0.05	N.m
Induced resistance (R)	63	Ω
Armature inductor (L)	27	mH
Moment of motor inertia (J)	0.000075	N.m ²
Electro motive force (E)	3.6	V/rad/s
Coefficient of fiction (Cf)	0.015	m.N.s/rad
Motor viscous friction (B)	1	N.m.s

TABLE 3
MODEL OF NO-LOAD DC WHEELS MOTOR CONTROL

No-Load dc wheels model motor control	Transfer function	Natural frequency	Damping ratio
	$Y = \frac{18}{s^2 + 15667s + 31111751}$	5578	1.4

function, the model of the direct current wheels control motor is deduced in Table 3.

The denominator of the transfer function of the system is in the form that implies that the damping ratio $\delta = 1.4 > 1$, meaning that the system is critically damped and presents no oscillations [49].

2) *Parameters of controller*

The parameters of the adaptive PID controller are deduced by comparing the closed-loop transfer function $G(s)$ with the transfer function of the second-order system as equation (37) [48], [49]:

$$G(s) = \frac{K_c \omega_n^2}{s^2 + 2\delta \omega_n s + \omega_n^2} \quad (37)$$

From equation (37), the controller parameters shown in Table 4, and determined by the Ziegler - Nichols method, we then have equation (38) [49]:

$$\begin{cases} K_p = 0.6K_c \\ K_i = \frac{2K_c}{T_c} \\ K_d = \frac{K_c T_c}{8} \\ \omega_n = \frac{2\pi}{T_c} \end{cases} \quad (38)$$

where:

- ω_n is the natural frequency (rad/s)
- T_c is the period of oscillations established at the critical gain (s)
- K_c is the critical gain ($K_c = 1$ for our case)

TABLE 4
PARAMETER OF THE CONTROLLER

Parameter	Value
Proportional parameter K_p	4
Integral parameter K_i	100
Derivative parameter K_d	0.00005
Mechanism adaptation parameter (γ)	1
Control parameter θ_1	1.29
Control parameter θ_2	0.93
Control parameter θ_3	0
Control parameter θ_0	1

3) Model reference parameters

The reference and projection models are selected because they possess the desired plant dynamics and remain unmodified throughout the experiment. Moreover, it is recommended to construct the projection model to be faster than the desired response. This is because the goal of the MRAC controller is to compel the plant to follow the reference model, and in any causal system, the plant's reaction always lags behind the response of the reference model. This can be easily accomplished by configuring the reference model with $\omega_n = 8.66 \text{ Kg/s}$ and $\delta = 1.15$ (where $\delta > 1$ indicates a damped reference model with no oscillations in its step response), as shown in table 5 [48].

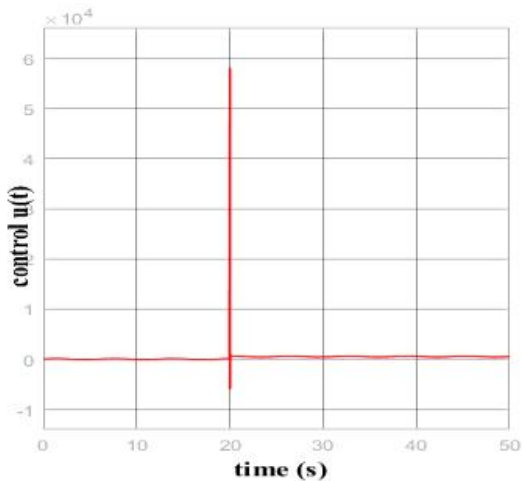
4) Simulation results without disturbances

a) Tracking the trajectory of the cleaner robot using step reference

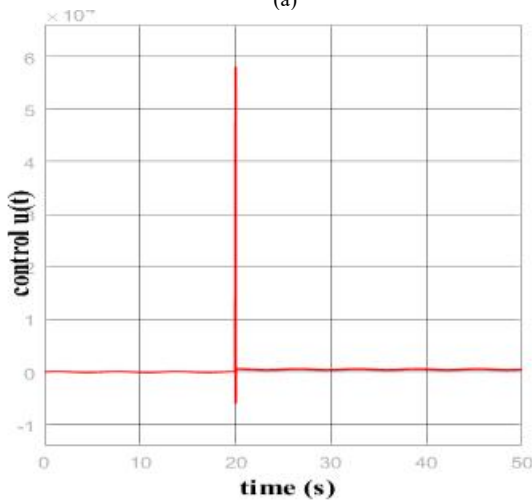
A reference to a step provides the distance between

TABLE 5
THE REFERENCE MODEL PARAMETERS

Reference Model	Transfer function	Natural frequency	Damping ratio
	$Y_m(s) = \frac{75}{s^2 + 20s + 75}$	8.66	1.15



(a)



(b)

Figure 8. Tracking control $u(t)$ of the cleaner robot using step reference: (a) PID algorithm and (b) MRAC algorithm without disturbances before 50s

two defined levels at a specific moment. When the control inputs are heavy steps, the step response of our cleaner robot is given an initial state that represents the time evolution of its outputs to clean the left and right sides of a solar panel at a particular time. The advantage of having a side brush is that the step reference establishes a path that enables the robot to move along the solar panels.

Figure 8 illustrates the control with the desired trajectory and no disturbance using the PID algorithm in 8(a) and the MRAC algorithm in 8(b). Figures 9 and 10 illustrate the tracking of the desired cleaning trajectory

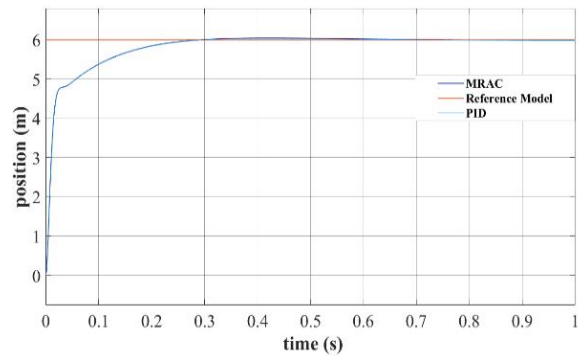
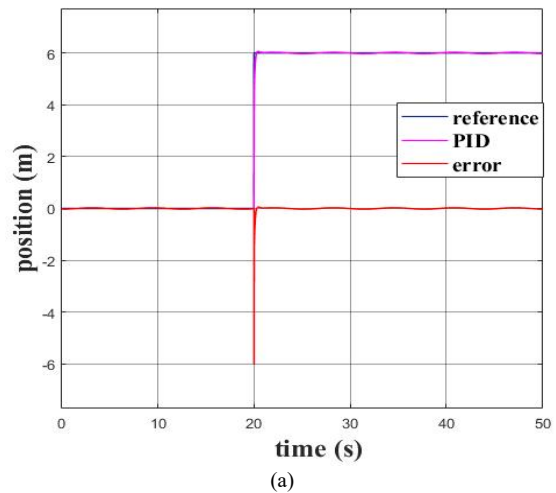
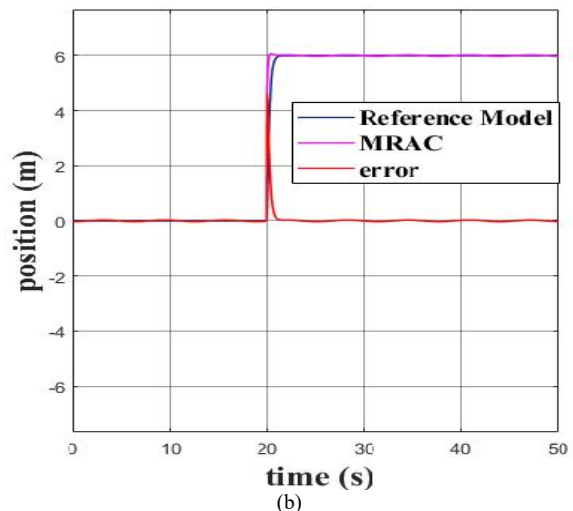


Figure 9. Tracking cleaning trajectory using PID algorithm and MRAC algorithm with a step desired trajectory without disturbances before 1s.



(a)



(b)

Figures 10. Tracking and error cleaning trajectory using PID algorithm 10(a) and MRAC algorithm 10(b) with a step desired trajectory without disturbances before 50s

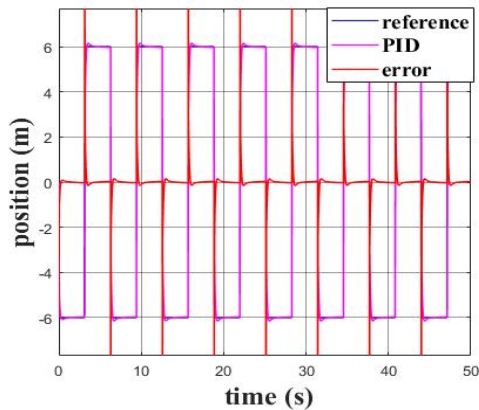
using step response without disturbance using the PID algorithm before 1 second in Figure 9, before 50 seconds in Figure 10(a), and the MRAC algorithm before 1 second in Figure 9, and before 50 seconds in Figure 10(b).

b) Tracking the trajectory of the cleaner robot using square wave reference

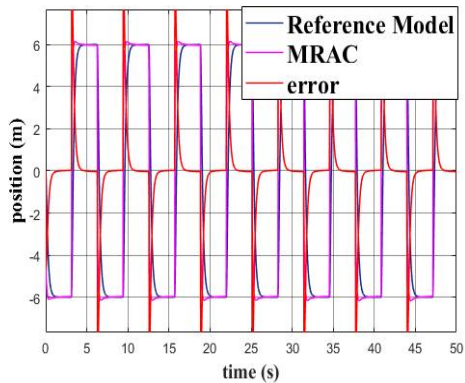
At regular intervals, a square wave reference generates square wave pulses. The square wave reference response of our cleaner robot enables us to determine the amplitude, pulse width, period, and phase delay of the cleaning trajectory. The goal is to clean the left and right, up and down, and vertical solar panels at regular intervals. Thanks to the square wave reference, the cleaner robot can move in a straight line, and upon completing its journey, it turns to align parallel to the previously traveled straight line. Figures 11(a) and 11(b) illustrate the tracking and error-cleaning trajectory using a square wave reference.

c) Evaluation of robustness of the proposed algorithm control

When performing the task of cleaning a solar panel, the vacuum cleaner robot may encounter measurement sensors for slippage, target location, velocity, and acceleration, as well as other disturbances such as noise, wind, rain, snow, and variable DC-DC motor parameters. White noise is used in this instance to represent all of these disturbances in the Matlab/Simulink software using step and square wave references. Figure 12 depicts white noise with a



(a)



(b)

Figure 11. Tracking trajectory of the cleaner robot and tracking error using square wave reference (a) PID algorithm and (b) MRAC algorithm without disturbances before 50s

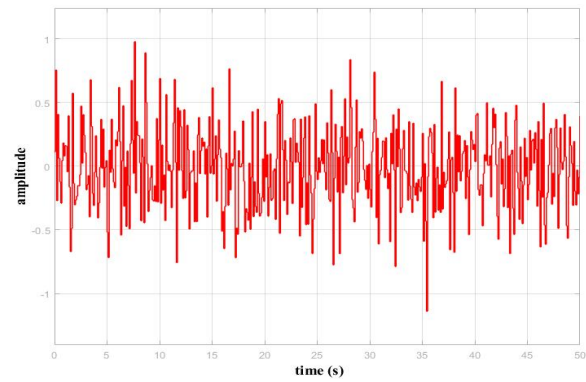


Figure 12. White noise at 1% before 50s

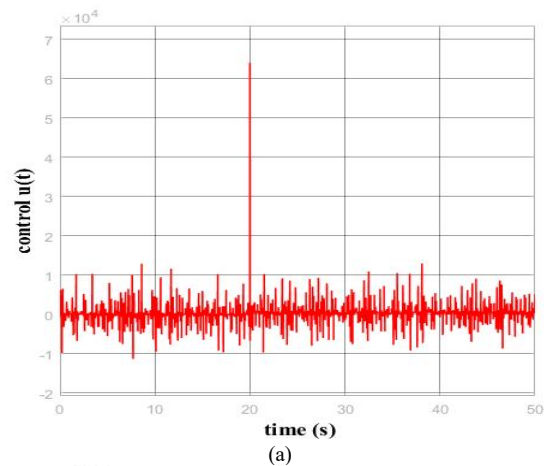
magnitude of 1% to indicate the disturbances before 50 s.

d) Case of small disturbances using step response

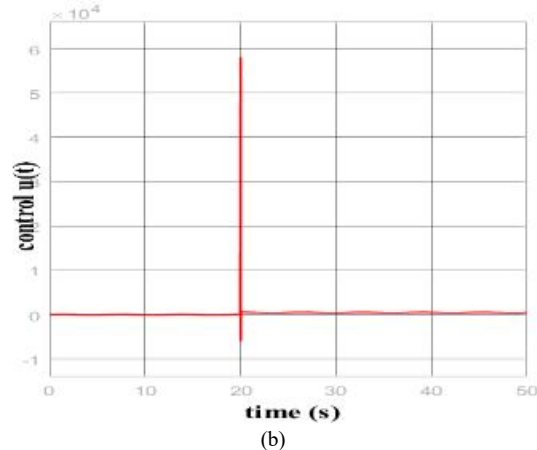
Figure 13 shows the control using PID algorithm 13(a) and MRAC algorithm 13(b) with a step-desired trajectory and disturbance at a 1% level before 50 s. Figures 14 and 15 illustrate the tracking of the desired cleaning trajectory using step response with disturbances at 1% level using the PID algorithm before 1 second in Figure 14, before 50 seconds in Figure 15(a), and the MRAC algorithm before 1 second in Figure 14, and before 50 seconds in Figure 15(b).

e) Case of small disturbances using square wave reference.

The solar panels are specifically designed for regular horizontal and vertical cleaning on the left and



(a)



(b)

Figure 13. Tracking control $u(t)$ of the cleaner robot using step reference (a) PID algorithm and (b) MRAC algorithm at 1% of disturbances before 50s

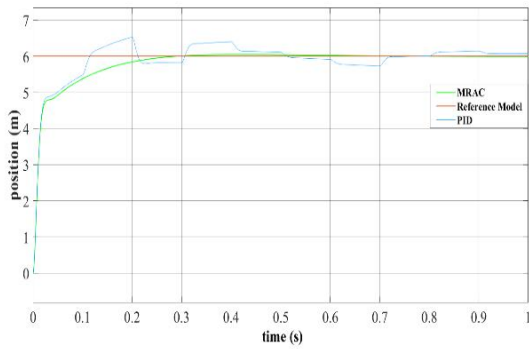


Figure 14. Tracking trajectory of the cleaner robot using step response reference at 1% of disturbances with PID algorithm and MRAC algorithm before 1s

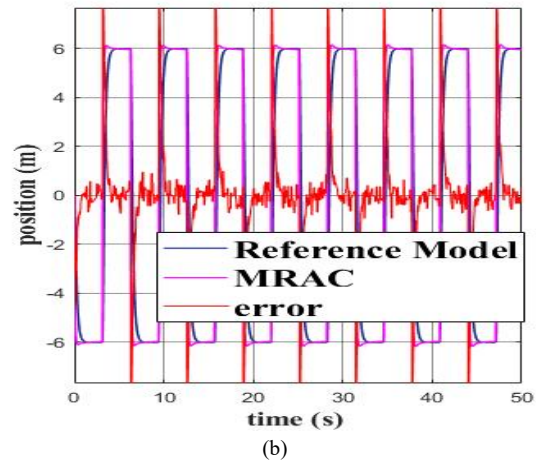
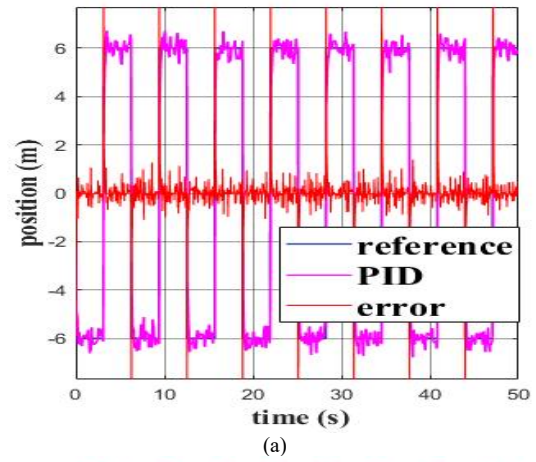


Figure 16. Tracking trajectory of the cleaner robot and tracking error using square wave reference at 1% of disturbances (a) PID algorithm and (b) MRAC algorithm before 50 s

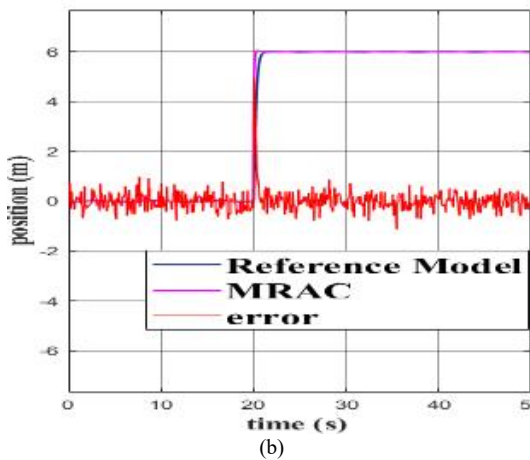
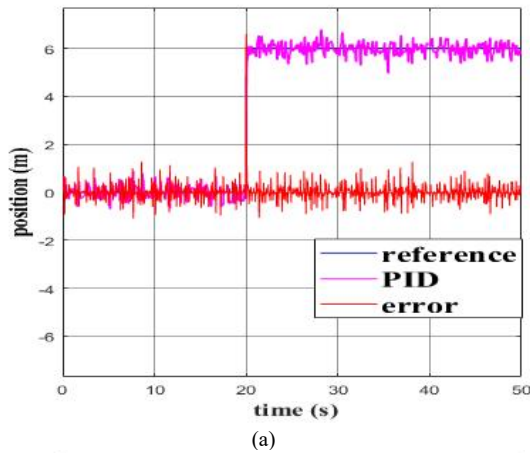


Figure 15. Tracking trajectory of the cleaner robot and tracking error using step reference at 1% of disturbances (a) PID algorithm and (b) MRAC algorithm before 50 s

right. Figures 16(a) and 16(b) illustrate the tracking trajectory using a square wave reference with 1% perturbations before 50 seconds.

f) Case of high disturbances using step reference

Figure 17 depicts the control system with a step-desired trajectory and a disturbance at a 60% level using the PID algorithm in 17(a) and the MRAC algorithm in 17(b).

To clean both the left and right solar panels horizontally, and considering disturbances at regular intervals, a tracking trajectory using both PID and MRAC algorithms is depicted in Figure 18(a) whereas Figure 18(b), is depicted the tracking trajectory errors.

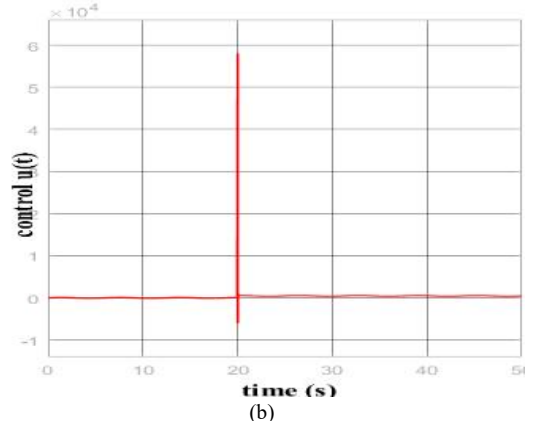
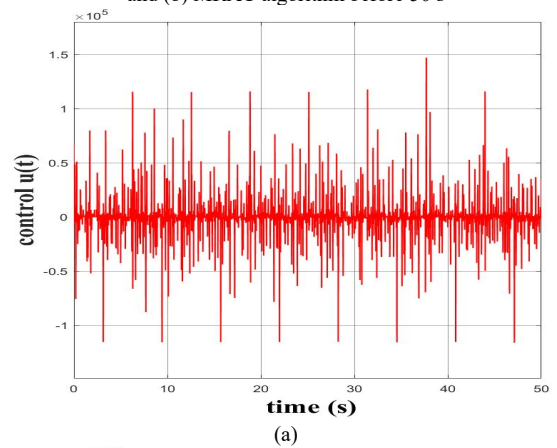


Figure 17. Tracking control $u(t)$ of the cleaner robot using step reference (a) PID algorithm and (b) MRAC algorithm at 60% of disturbances before 50 s

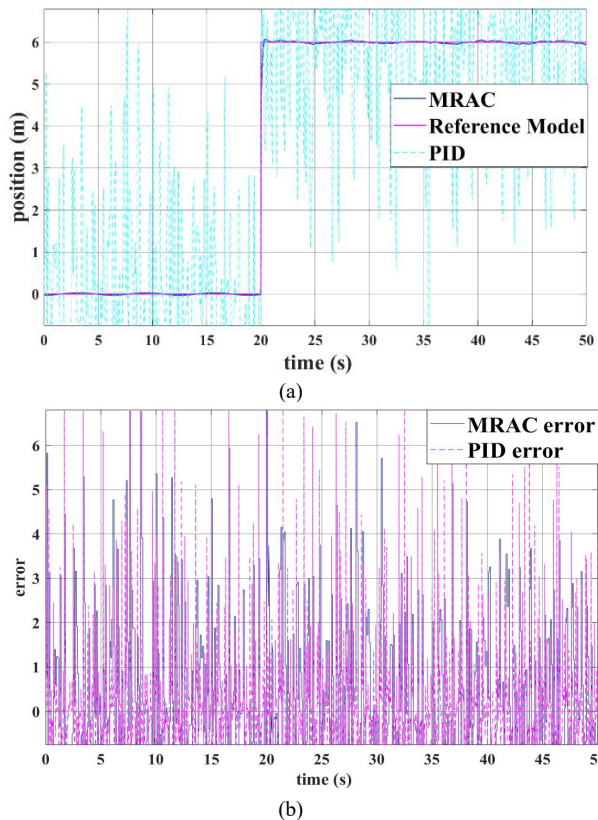


Figure 18. PID and MRAC algorithms with step reference at 60% of disturbances before 50 s used for (a) tracking trajectory of the cleaner robot and (b) tracking position error

The trajectory utilizes a step reference (Refer to Figure 18) at disturbances of 60% level.

g) *Case of high disturbances using square reference*

The left and right solar panels are meant to be regularly cleaned both horizontally and vertically. The tracking trajectory, utilizing a square wave reference with 60% of disturbances before 50 seconds, both using PID and MRAC algorithms is shown in Figure 19(a) and the tracking cleaning trajectory errors is shown in Figure 19(b).

h) *Dynamic qualitative comparative of the control of tracking cleaning trajectory algorithms*

The qualitative dynamic performance of the PID and MRAC algorithms is displayed in Table 6. From the table, it is evident that both algorithms ensure the stability of the vacuum cleaner robot without interruption. However, in terms of response time, tracking the cleaning trajectory in the presence of disturbances, cleaning solar panels in the face of disturbances, energy losses, and the efficiency of PV systems, as well as the accuracy of tracking the desired cleaning trajectory of PV systems, the proposed MRAC control algorithm outperforms the PID control algorithm. The proposed MRAC approach exhibits a tracking cleaning error that tends toward zero even in the presence of disturbances, demonstrating excellent performance in tracking the desired cleaning trajectory. It has a medium complexity and is robust against uncertainties or variable parameters, noise, and

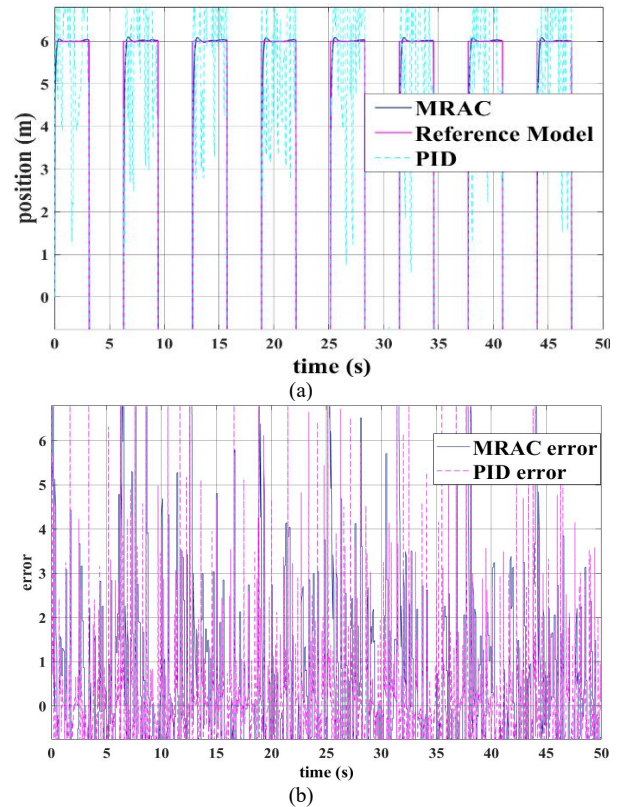


Figure 19. PID and MRAC algorithms with square reference at 60% of disturbances before 50 s used for (a) Tracking trajectory of the cleaner robot and (b) tracking position error

measurement sensor errors such as slip, target position, velocity, and acceleration.

i) *Dynamic quantitative Comparative of the control of tracking cleaning trajectory*

The quantitative dynamic performance of the PID and MRAC algorithms is displayed in Table 7 by following the trajectory position error of the tracking cleaning trajectory of the cleaner robot. From the table, it is evident that both algorithms ensure the tracking of

TABLE 6
DYNAMIC QUALITATIVE ANALYSIS OF THE TRACKING CLEANING TRAJECTORY ALGORITHMS

Criteria for Evaluation	PID [4]	MRAC
Stability without disturbances	Guarantee	Guarantee
Stability in face of disturbances	No	Guarantee
Time of calculations	High	Low
Number of sensors	More	Less
Energy consumption	Medium	Low
Complexity	Low	Medium
Cleaning error with no disturbances	Zero	Zero
Cleaning error with disturbances	High	Zero
Robustness	No	Yes
Speed of convergence	Fast	Very Fast
Flexibility	Yes	Yes
Accuracy without disturbances	High	High
Accuracy with disturbances	Weak	High

TABLE 7
POSITION ERROR AND TIME RESPONSE OF THE TRACKING
CLEANING TRAJECTORY OF THE CLEANER ROBOT

Error/Time response	PID [4]	MRAC	Reference
Error without disturbances	0	0	Step and Square
Error at 1 % of disturbances	1.6	0.3	Step
Error at 1% of disturbances	1.5	0.1	Square
Error at 60 % of disturbances	3.9	0.9	Step
Error at 60 % of disturbances	3.8	0.6	Square
Time response without disturbances	0.28 s	0.28 s	Step
Time response with 1 % of disturbances	0.51 s	0.28 s	Step

the cleaning trajectory without disturbances (that is the reason why the value of their position tracking cleaning trajectory error is equal to zero), but in the presence of disturbances, the PID algorithm presents a big difficulty to follow the desired cleaning trajectory with a position-tracking cleaning trajectory error more than three. In the presence of disturbances, the best reference for tracking the cleaning trajectory both with PID and MRAC algorithms is the square reference. The MRAC approach presents the difficulty of following the desired cleaning trajectory in the face of high disturbances.

Figure 20 is a histogram representing the comparison of PID and MRAC algorithms through the position error of the desired cleaning trajectory of the cleaner without disturbances, at 1%, and 60% of disturbances with step reference. According to Figure 18, the position error with the PID algorithm of the tracking of the desired cleaning trajectory is the same as the position error using the MRAC approach suggested without disturbances, but the position error with the PID algorithm of the tracking of the desired cleaning trajectory is higher than the position error using the

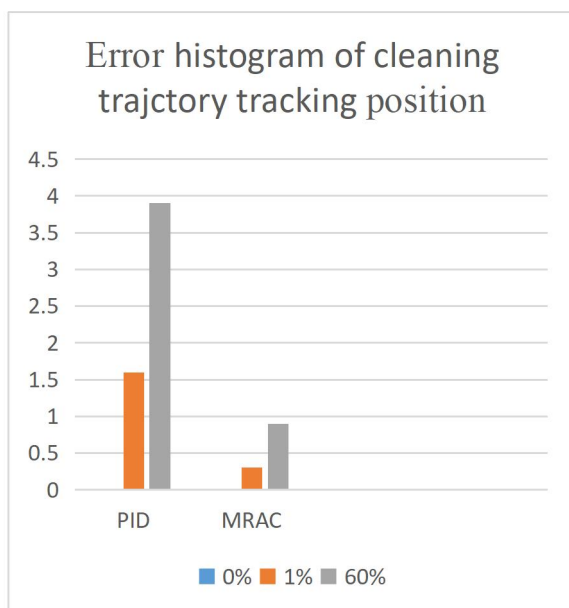


Figure 20. Comparative analysis of position error of tracking cleaning trajectory of the cleaner robot between PID and MRAC algorithms with step reference

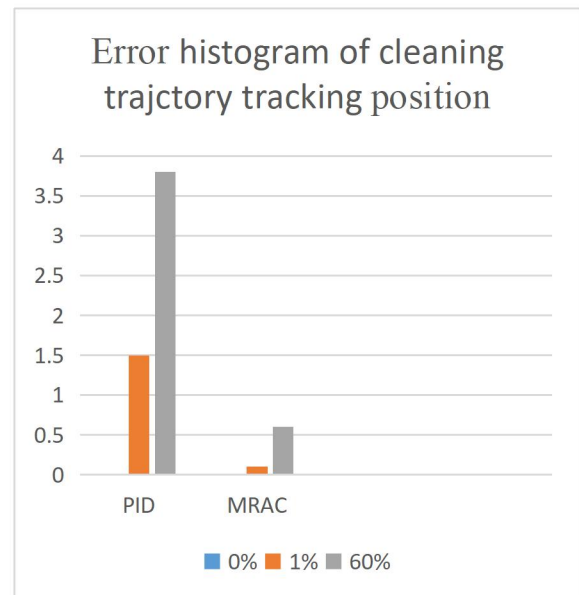


Figure 21. Comparative analysis of position error of tracking cleaning trajectory of the cleaner robot between PID and MRAC algorithms with square reference

proposed MRAC in face of disturbances when using step reference.

Figure 21 is a histogram representing the comparison of PID and MRAC algorithms through the position error of the tracking of the desired cleaning trajectory of the cleaner without disturbances, at 1%, and 60% of disturbances with square reference. According to Figure 21, the position error with the PID algorithm of the tracking of the desired cleaning trajectory is the same as the position error using the MRAC approach suggested without disturbances, but the position error with the PID algorithm of the tracking of the desired cleaning trajectory is higher than the position error using the proposed MRAC in face of disturbances when using square reference.

B. Discussion

Figure 8 depicts the behavior of our vacuum cleaning robot's control using step response, without disturbances, to demonstrate the efficacy of the suggested MRAC algorithm. Figure 8(a) demonstrates that the control tends toward zero when employing the PID algorithm, but is only affected by the changing step at 20 seconds. Similarly, Figure 8(b) shows that the control tends toward zero when employing the MRAC method, but is only affected by the changing step at 20 seconds. The steady tracking trajectory of the robot is indicated by the control's tendency to zero.

Figures 9 allows us to evaluate the time response of the solar panels cleaning robot before 1 second for the desired cleaning trajectory following the PID algorithm and the proposed MRAC approach without disturbances. We observe that the time response of the solar panels cleaning robot is 0.28 seconds when using the PID algorithm, which is the same as that achieved with the proposed MRAC approach. The fact that the cleaning robot has a low time response allows it to consume less energy consumption from the solar panels.

Figures 10 and 11 demonstrate the tracking and error cleaning trajectories using the PID algorithm (10(a) and 11(a)) respectively and MRAC algorithm (10(b)

and 11(b)) respectively with a step and square response trajectory respectively before 50 seconds, without disturbances, when cleaning the solar panels with the vacuum cleaner robot. Both figures 10 and 11 show that the tracking cleaning trajectory is perfect, regardless of whether the PID or MRAC control algorithm is used, except for the changing step at 20 seconds where the system is slightly affected. The error tracking cleaning trajectory, which also tends toward zero, confirms the perfection of the tracking cleaning trajectory.

Figures 9, 10, and 11 demonstrate that regardless of whether the PID or MRAC algorithm is used, the vacuum cleaner robot's path-tracking motion is accurate and exhibits strong control performance while cleaning the solar panels. Proper cleaning of solar panels maximizes energy production, which can improve return on investment and extend the lifespan of the solar panels.

Figure 12 depicts white noise at a 1% level of disturbance to demonstrate the efficiency and robustness of the proposed MRAC algorithm before 50 seconds. The disturbances in this case may include noise, variable uncertainties, uncertain parameter values, measurement sensor slip errors, target location, velocity, and acceleration.

In Figure 13(a), the cleaning tracking trajectory of the vacuum cleaner robot is affected by the PID control algorithm, not tending toward zero, with only a 1% level of disturbances when using the step response before 50 seconds. This can result in more hot spots caused by dust collection, permanently harming PV cells and lowering the output power delivered by PV generators. Figure 13(b) demonstrates that the control still moves toward zero when employing the MRAC method, with the changing step at 20 seconds being the sole factor that affects it. The tracking trajectory of the robot remains steady, indicated by the control's tendency to zero before 50 seconds.

Figure 14 allows us to evaluate the time response of the solar panels cleaning robot before 1 second for the desired cleaning trajectory following the PID algorithm and the proposed MRAC approach with 1% level of disturbances. We observe that the time response of the solar panels cleaning robot is 0.51 seconds when using the PID algorithm, and stay 0.28 seconds when using the MRAC proposed approach. The low value of time response using MRAC proposed approach than this using PID algorithm allows a low consumption of the energy of the cleaner robot when using MRAC proposed approach.

Figures 15(a) and 16(a) respectively show that the cleaning trajectory utilizing the PID algorithm with step and square reference respectively before 50 seconds does not follow the required cleaning trajectory and its tracking error does not tend to zero, even with a 1% level of disturbances. This can cause a loss in PV efficiency and long-term damage to PV cells. In contrast, Figures 15(b) and 16(b) respectively demonstrate that the cleaning trajectory utilizing the MRAC proposed approach with step and square reference respectively before 50 seconds continues to follow the planned cleaning trajectory and its tracking error tends toward zero, even with a 1% level of disturbances. Achieving

the intended cleaning trajectory with the vacuum cleaner robot can lead to an increase in PV efficiency.

The MRAC algorithm significantly enhances the robustness and accuracy of the system, while reducing the number of sensors and errors during the cleaning of solar panels, even in presence of the disturbances. To achieve excellent tracking performance and improve flexibility and robustness, it is crucial to minimize the tracking cleaning error. The MRAC approach can be applied to handle bounded parameter uncertainties and bounded external disturbances. Poor cleaning of solar panels using the PID approach in the presence of 1% of disturbances can reduce the amount of sunlight that reaches the PV cells due to dust accumulation, leading to a significant decrease in efficiency and energy production.

Figure 17 illustrates how the control is more sensitive to high disturbances when using the PID algorithm (Figure 17(a)) with step response before 50 seconds, which is used to demonstrate the robustness of the proposed MRAC method. The cleaning tracking trajectory of the vacuum cleaner robot can be significantly more impacted, not tending toward zero, with a 60% level of disturbances. However, the control still moves toward zero when employing the MRAC algorithm (Figure 17(b)), with the changing step at 20 seconds being the only factor affecting it. The robot's tracking trajectory remains steady, and the suggested algorithm remains robust, even in the presence of a significant disturbance at a 60% level, due to the control's tendency to zero.

In Figure 18(a) and 19 (a) respectively, using the step and square response respectively before 50 seconds, it is demonstrated that the cleaning trajectory using the PID algorithm does not significantly match the planned cleaning trajectory and their tracking cleaning position error (see Figures 18(b) and 19(b)) does not tend substantially toward zero when considering 60% level disturbances. This can lead to reduced efficiency of PV systems and permanent harm to PV cells. Figures 18(b) and 19(b) demonstrate that the cleaning trajectory utilizing the MRAC proposed approach still follows the planned cleaning trajectory, and its tracking error tends toward zero, even with a 60% level of disturbances before 50 seconds. This highlights the robustness of the MRAC proposed approach in maintaining accurate tracking performance, even under high disturbances.

Figures 20 and 21 show that the position error with the MRAC algorithm for tracking the desired cleaning trajectory becomes high when the disturbances become very high using step and square reference, but less than the position error with the PID algorithm for tracking the desired cleaning trajectory. According to Figures 20 and 21, the best reference to track the cleaning trajectory is the square reference in the presence of disturbances.

Overall, the presented figures demonstrate that the MRAC algorithm outperforms the PID algorithm in terms of accuracy, robustness, and tracking performance when cleaning solar panels with a vacuum cleaner robot. The MRAC algorithm shows superior control behavior, minimizing tracking errors and maintaining precise cleaning trajectories, even in the presence of

disturbances. This enhanced performance can lead to improved efficiency of PV systems, reduction of PV panel power losses, reduction of the number of used sensors in the PV systems, cleanliness of solar panels, reduction of the energy consumption by the cleaner panel robot, and protection of the PV cells, ultimately resulting in higher power output from solar panels. Robotic cleaning is better than chemical cleaning, which is harmful to the environment. Using the PID approach, weather conditions such as rain, wind, and snow-considered disturbances can influence the frequency and method of cleaning by the robotic cleaner, affecting cleaning efficiency and solar panel performance. The proposed MRAC approach for managing robotic cleaner in real time, taking disturbances into account, can improve overall efficiency. Robotic cleaning can also be used in arid regions that require large amounts of water for cleaning.

IV. CONCLUSION

The paper deals with the optimal tracking of the desired cleaning trajectory, and maximizing the efficiency of solar panels by mobile robotic solar panel cleaners in the presence of disturbances. To achieve this, we started by presenting the effects of dust deposits on solar panels in the literature review. Solar panel cleaning methods have also been presented. Among these methods, the control algorithms for trajectory tracking of solar panel cleaning robots have been presented. We took as a case study example, as we could do with any solar panel cleaning robot, the mobile solar panel cleaning robot presented in the work of Aravind et al. The mathematical modeling of the robot from the work of Aravind et al has been done, more precisely that of the wheel control motors of the robot for tracking the desired cleaning trajectory of the solar panels. The stability of the cleaning system has been demonstrated by the Lyapunov law. The numerical simulation results were obtained via the Matlab/Simulink environment, and the white noise of this Matlab environment was used as a disturbance to the cleaning robot.

The simulation results obtained by the proposed MRAC approach were compared to those obtained by the PID algorithm presented in the literature. Based on the parameter of tracking error and convergence time of the desired cleaning trajectory of the solar panels, the proposed MRAC approach is seen to be better for optimal tracking of the desired cleaning trajectory of the solar panels by a mobile cleaning robot and the smallest time response compared to the tracking errors and the time response obtained by the PID algorithm presented in the literature. These tracking errors of the desired cleaning trajectory of the solar panels are of 0.28 minimum for the proposed MRAC approach and 0.51 for the PID algorithm in the presence of a minimum disturbance of 1%.

The iRobot solar panel cleaning robot, developed by Aravind et al. And, used for our work, has a mass of 1.5 kg, and operates at a power of 250 W. It can clean approximately 930 solar panels from the Kyocera Solar KC 130 GT module, which has dimensions of 1.425 m in length and 0.652 m in width. The iRobot operates

under a working voltage of 12 V DC, at a frequency of 50 Hz, and uses a 12.6 V DC battery, 100 AH, capable of supporting a current of 20 A and taking approximately 5 hours to charge. It covers an area of 864 m² and cleans a surface area of 0.06 m² in one second. Our work can address several cleaning problems faced by solar panels, including difficult access, risk of damage, weather conditions, accumulation of dirt, cleaning frequency, use of chemicals, cleaning efficiency, automation of the cleaning system, water usage, and safety.

The use of the MRAC approach for optimal tracking of the desired cleaning trajectory of solar panels via a mobile solar panel cleaning robot can significantly and effectively increase the production of any PV system extending its lifespan, avoid the damage of PV cells during the cleaning process, minimize maintenance costs, reduce solar panels power losses, reduce human efforts, reduce the number of sensors used, improve the time response of the cleaner robot in presence of disturbances and reduce the complexity of the control algorithms used in these systems for control of the desired cleaning trajectory tracking of the cleaning robot, and allow dynamic adaptation to varying external conditions, thereby ensuring a consistent performance level of the solar panels. However, we can highlight certain limits of the proposed MRAC approach such as it is more complex than some algorithms presented in the literature, particularly, the proportional integral derivative algorithm. Another limitation of this MRAC approach is its sensitivity to very large disturbances. As a perspective for our future work, we plan to experimentally test the proposed MRAC algorithm on the cleaning robot presented in the work of Aravind et al, or on any solar panel cleaning robot.

DECLARATIONS

Conflict of Interest

There is no competing interest for all authors of this manuscript research.

CRedit Authorship Contribution

Yves Abessolo Mindzie: Conceptualization, Methodology, Software, Visualization, Investigation, Writing-Reviewing and Editing; Joseph Kenfack: Supervision, Writing-Original draft preparation; Brice Ekobo Akoa: Visualization, Investigation, Reviewing; Noé Paulin Frederick Ntomba: Visualization, Investigation, Writing-Reviewing and Editing; Blaise Njoya Fouedjou: Data curation; Guy M. Toche Tchio: Writing-Reviewing; Joseph Voufo: Supervision, Reviewing; Urbain Nzotcha: Supervision, Reviewing;

Funding

This research did not receive any specific grant from funding agencies in the public, commercial or not-for-profit sectors. "The author(s) received no financial support for the research, authorship, and/or publication of this article."

Acknowledgment

We extend our heartfelt gratitude to the Director and the Head of Ph.D. students at the Laboratory of Small Hydro and Hybrid Systems, National Advanced School of Engineering, Yaoundé, for their invaluable support in facilitating our

research. Our appreciation also goes to the Head of the Laboratory of Energy, Water, and Environment at the same institution, as well as all the faculty members and the Ph.D. student from the Fab Lab Renewable Energy Laboratory at the National Advanced School of Engineering, University of Yaoundé I, Cameroon, for their contributions to our research.

Abbreviations

<i>PV</i>	Photovoltaic
<i>PID</i>	Proportional Integral Derivative
<i>SPV</i>	Solar Photovoltaic
<i>MRAC</i>	Model Reference Adaptive Control
<i>FLC</i>	Fuzzy Logic Controller
<i>MPC</i>	Model Predictive Control
$Re = r$	Stator resistance (Ω)
$i_e = i$	Inductor current (A)
I	Rotor current (A)
Φ	Magnetic flux (Wb)
$B = Bm$	Motor viscous friction (N.m.s)
θ	Position (m or rad)
$V_s = V_e = V_b$	Stator voltage (V)
$U_a = U$	Rotor voltage (V)
$R_a = R$	Rotor resistance (Ω)
$J = Jm$	Moment of motor inertia (Kg.m ²)
$K = K_b = K_a$	Motor torque (N.m)
$L = L_a = L_e$	Electric inductance (H)

REFERENCES

- [1] S. C. S. Costa, A. S. A. C. Diniz, and L. L. Kazmerski, "Solar Energy Dust and Soiling R&D Progress: Literature review update for 2016," *Renew. Sustain. Energy Rev.*, vol. 82, 2018, doi: 10.1016/j.rser.2017.09.015.
- [2] D. Deb and N. L. Brahmabhatt, "Review of Yield Increase of Solar Panels Through Soiling Prevention, and a Proposed Water-Free Automated Cleaning Solution," *Renew. Sustain. Energy Rev.*, vol. 82, no. April, pp. 3306–3313, 2018, doi: 10.1016/j.rser.2017.10.014.
- [3] V. M. Mbachau, A. G. Muogbo, O. S. Ezeanaka, E. O. Ejchukwu, and T. D. Ekwunife, "An Economic Based Analysis of Fossil Fuel Powered Generator and Solar Photovoltaic System as Complementary Electricity Source For a University Student's Room," *J. Sol. Energy Res.*, vol. 7, no. 4, pp. 1159–1173, 2022, doi: 10.22059/jser.2021.332724.1225.
- [4] G. Aravind, G. Vasani, T. S. B. G. Kumar, R. N. Balaji, and G. S. Ilango, "A Control Strategy for an Autonomous Robotic Vacuum Cleaner for Solar Panels," *Proc. - 2014 Texas Instruments India Educ. Conf. TIIEC 2014*, pp. 53–61, 2017, doi: 10.1109/TIIEC.2014.018.
- [5] Mircea Neagoe and Bogdan Burduhos, "Comparative Performance Analysis of Solar Tracking System Types at Different Latitudes," *J. Sol. Energy Res. Updat.*, vol. 8, no. March 2021, pp. 1–10, 2021, doi: 10.31875/2410-2199.2021.08.1.
- [6] H. Babazadeh and S. Javan, "Solar Panel Efficiency Enhancement using Water Filter," *J. Sol. Energy Res.*, vol. 6, no. 4, pp. 883–886, 2021.
- [7] S.D. Farahani, M. Alibeigi, "Investigation of Power Generated From a Pvt-Teg System in Iranian Cities" *J. Sol. Energy Res.*, November, 2020, doi: 10.22059/JSER.2020.308162.1170.
- [8] N. Ghaffarzadeh and A. Azadian, "A Comprehensive Review and Performance Evaluation in Solar (Pv) Systems Fault Classification and Fault Detection Techniques," *J. Sol. Energy Res.*, vol. 4, no. 4, pp. 252–272, 2019, [Online]. Available: <https://jser.ut.ac.ir/article/74001.html>
- [9] B. Mehimmedetsi and R. Chennai, "Modelling of DC PV System with MPPT," *Proc. 2015 IEEE Int. Renew. Sustain. Energy Conf. IRSEC 2015*, no. December 2015, 2016, doi: 10.1109/IRSEC.2015.7455013.
- [10] R. Martinez-Guerra and J. De Leon-Morales, "On Nonlinear Observers," *IEEE Conf. Control Appl. - Proc.*, no. July, pp. 324–328, 1997, doi: 10.1201/b10384-41.
- [11] U. Nzotcha, J. Kenfack, and M. Blanche Manjia, "Integrated Multi-Criteria Decision Making Methodology for Pumped Hydro-Energy Storage Plant Site Selection from a Sustainable Development Perspective With an Application," *Renew. Sustain. Energy Rev.*, vol. 112, no. May, pp. 930–947, 2019, doi: 10.1016/j.rser.2019.06.035.
- [12] Y. Ma, Y. Zhao, R. Jia, W. Wang, and B. Zhang, "Impact of Financial Development on The Energy Intensity of Developing Countries," *Heliyon*, vol. 8, no. 8, 2022, doi: 10.1016/j.heliyon.2022.e09904.
- [13] IEA, "World Energy Investment 2023," <https://www.iea.org/reports/world-energy-investment-2023>, 2023.
- [14] J. Kenfack, O. V. Bossou, J. Voufo, and S. Djom, "Addressing the Current Remote Area Electrification Problems with Solar and Microhydro Systems in Central Africa," *Renew. Energy*, vol. 67, pp. 10–19, 2014, doi: 10.1016/j.renene.2013.11.044.
- [15] W. Huang, K. Zhou, K. Sun, and Z. He, "Effects of Wind Flow Structure, Particle Flow and Deposition Pattern on Photovoltaic Energy Harvest Around a Block," *Appl. Energy*, vol. 253, no. July, p. 113523, 2019, doi: 10.1016/j.apenergy.2019.113523.
- [16] F. A. Almalki, A. A. Albraikan, B. O. Soufiene, and O. Ali, "Utilizing Artificial Intelligence and Lotus Effect in an Emerging Intelligent Drone for Persevering Solar Panel Efficiency," *Wirel. Commun. Mob. Comput.*, vol. 2022, 2022, doi: 10.1155/2022/7741535.
- [17] J. Farrokhi Derakhshandeh *et al.*, "A Comprehensive Review of Automatic Cleaning Systems of Solar Panels," *Sustain. Energy Technol. Assessments*, vol. 47, no. July, p. 101518, 2021, doi: 10.1016/j.seta.2021.101518.
- [18] H. Zhen-Yu *et al.*, "Research of Control System Based on Solar Panel Cleaning Mechanism," *Int. J. Res. Eng. Sci. ISSN*, vol. 4, no. 5, pp. 1–05, 2016, [Online]. Available: www.ijres.org
- [19] Z. A. Darwish, H. A. Kazem, K. Sopian, M. A. Al-Goul, and H. Alawadhi, "Effect of Dust Pollutant Type on Photovoltaic Performance," *Renew. Sustain. Energy Rev.*, vol. 41, pp. 735–744, 2015, doi: 10.1016/j.rser.2014.08.068.
- [20] P. R. Satpathy, S. Jena, and R. Sharma, "Power Enhancement from Partially Shaded Modules of Solar Pv Arrays Through Various Interconnections Among Modules," *Energy*, vol. 144, pp. 839–850, 2018, doi: 10.1016/j.energy.2017.12.090.
- [21] A. Kasaeian, G. Nouri, P. Ranjbaran, and D. Wen, "Solar Collectors and Photovoltaics as Combined Heat and Power Systems: a Critical Review," *Energy Convers. Manag.*, vol. 156, no. November 2017, pp. 688–705, 2018, doi: 10.1016/j.enconman.2017.11.064.
- [22] S. Cai *et al.*, "Parameters Optimization of the Dust Absorbing Structure for Photovoltaic Panel Cleaning Robot Based on Orthogonal Experiment Method," *J. Clean. Prod.*, vol. 217, pp. 724–731, 2019, doi: 10.1016/j.jclepro.2019.01.135.
- [23] H. Kawamoto and T. Shibata, "Electrostatic Cleaning System For Removal of Sand from Solar Panels," *J. Electrostat.*, vol. 73, pp. 65–70, 2015, doi: 10.1016/j.elstat.2014.10.011.
- [24] Y. B. Park, H. Im, M. Im, and Y. K. Choi, "Self-Cleaning Effect of Highly Water-Repellent Microshell Structures for Solar Cell Applications," *J. Mater. Chem.*, vol. 21, no. 3, pp. 633–636, 2011, doi: 10.1039/c0jm02463e.
- [25] S. R. Bhandari *et al.*, "Performance Analysis of Semi-Automatic Solar Panel Cleaning System," *OCEM J. Manag. Technol. Soc. Sci.*, vol. 3, pp. 110–116, 2024, DOI: <https://doi.org/10.3126/ocemjmtss.v3i1.62230>
- [26] V. Bedge, A. More, O. Gholap, S. Maharnur, and P. Patil, "Automatic Solar Panel Cleaning Robot Using Arduino," *Int. Res. J. Mod. Eng. Technol. Sci.*, no. 05, pp. 5335–5337, 2024.
- [27] G. Ashwini, T. S. Ravichandran, S. R. A. S, and S. P. K, "Robot for Cleaning Solar Panels with Automated Functionality," *Int. Res. J. Eng. Technol.*, pp. 1552–1555, 2024.
- [28] G. Zubi, R. Dufo-López, G. Pasaoglu, and N. Pardo, "Techno-Economic Assessment of an Off-Grid PV System for Developing Regions to Provide Electricity for Basic Domestic Needs: a 2020–2040 Scenario," *Appl. Energy*, vol. 176, no. 2016, pp. 309–319, 2016, doi: 10.1016/j.apenergy.2016.05.022.
- [29] P. T. K and B. P. Tushar, "Autonomous Solar Panel Cleaning Robot," *Int. J. Adv. Res. Sci. Commun. Technol.*, pp. 417–420, 2024, doi: 10.48175/IJARSCT-15459.
- [30] A. Chellal and A. I. Pereira, "Innovative Robot Design for Cleaning Solar Panels," *Proc. 11th Int. Conf. Simul. Model. Methodol. Technol. Appl. (SIMULTECH)*, pp. 264–270, 2021, doi: 10.5220/0010540102640270.
- [31] R. Kumar, P. S. Ramaprabha, S. R. Kishore, and S. Jayanthi, "Automatic Solar Panel Cleaner Robot using IoT," *Journal of Physics: Conference Series*, vol. 1964, no. 6, p. 062084, Jul. 2021. doi: 10.1088/1742-6596/1964/6/062084.
- [32] M. Zolfaghari, S. H. Hosseinian, S. H. Fathi, M. Abedi, and G. B. Gharehpetian, "A New Power Management Scheme for

- Parallel-Connected PV Systems in Microgrids,” *IEEE Trans. Sustain. Energy*, vol. 9, no. 4, pp. 1605–1617, 2018, doi: 10.1109/TSTE.2018.2799972.
- [33] H. R. Baghaee, M. Mirsalim, and G. B. Gharehpetian, “Multi-Objective Optimal Power Management and Sizing of a Reliable Wind/PV Microgrid with Hydrogen Energy Storage Using Mopso,” *J. Intell. Fuzzy Syst.*, vol. 32, no. 3, pp. 1753–1773, 2017, doi: 10.3233/JIFS-152372.
- [34] A. Al Shehri, B. Parrott, P. Carrasco, H. Al Saiari, and I. Taie, “Impact of Dust Deposition and Brush-Based Dry Cleaning on Glass Transmittance for PV Modules Applications,” *Sol. Energy*, vol. 135, pp. 317–324, 2016, doi: 10.1016/j.solener.2016.06.005.
- [35] C. Mehdipour and F. Mohammadi, “Design and Analysis of a Stand-Alone Photovoltaic System for Footbridge Lighting,” *J. Sol. Energy Res.*, vol. 4, no. 2, pp. 85–91, 2019, doi: 10.22059/jser.2019.283926.1120.
- [36] V. Soori, A. Ketabi, and A. H. Niasera, “Control of Three-Phase Buck-Type Dynamic Capacitor Using the Model Predictive Control Method for Dynamic Compensation of the Reactive Power and Load Current Harmonics,” *J. Solar Energy Res.*, vol. 6, no. 4, pp. 898–912, 2021, doi: 10.22059/jser.2021.313910.1185.
- [37] V. Janamala, “A New Meta-Heuristic Pathfinder Algorithm for Solving Optimal Allocation of Solar Photovoltaic System in Multi-Lateral Distribution System For Improving Resilience,” *SN Appl. Sci.*, vol. 3, no. 1, pp. 1–17, 2021, doi: 10.1007/s42452-020-04044-8.
- [38] E. Najafi, R. Rajabi, and N. Bayat, “Fault Tolerant Multilevel Inverter using Artificial Neural Network,” *J. Sol. Energy Res.*, vol. 9, no. 1, pp. 1745–1752, 2024, doi: 10.22059/jser.2024.359461.1309.
- [39] H. A. Van Essen and H. Nijmeijer, “Non-Linear Model Predictive Control for Constrained Mobile Robots,” *2001 Eur. Control Conf. ECC 2001*, pp. 1157–1162, 2001, doi: 10.23919/ecc.2001.7076072.
- [40] H. Y. Liu, “Design and Implementation of an Intelligent Cleaning Robot Based on Fuzzy Control,” *Adv. Mater. Res.*, vol. 1003, pp. 221–225, 2014, doi: 10.4028/www.scientific.net/AMR.1003.221.
- [41] G. Vachtsevanos, “Large-Scale Systems: Modeling, Control, And Fuzzy Logic: Mohammad Jamshidi; Prentice-Hall PTR, Englewood Cliffs, NJ, 1997, ISBN 0-13-125683-1,” *Automatica*, vol. 37, pp. 1500–1502, Jan. 2001.
- [42] F. Fang, “Design and Research of Cleaning Robot Based on Isc Algorithm,” *Acad. J. Manuf. Eng.*, vol. 17, no. 4, pp. 46–51, 2019.
- [43] L. Zhou and W. Li, “Adaptive Artificial Potential Field Approach for Obstacle Avoidance Path Planning,” *Proc. - 2014 7th Int. Symp. Comput. Intell. Des. Isc. 2014*, vol. 2, no. 1, pp. 429–432, 2015, doi: 10.1109/ISCID.2014.144.
- [44] B. Belobomevo, M. R. Saad, and R. Fareh, “Adaptive Sliding Mode Control of Wheeled Mobile Robot With Nonlinear Model And Uncertainties,” *Can. Conf. Electr. Comput. Eng.*, vol. 2018-May, no. January, pp. 1–5, 2018, doi: 10.1109/CCECE.2018.8447570.
- [45] V. Sathiyaa, M. Chinnadurai, S. Ramabalan, and A. Appolloni, “Mobile Robots and Evolutionary Optimization Algorithms for Green Supply Chain Management in a Used-Car Resale Company,” *Environ. Dev. Sustain.*, vol. 23, no. 6, pp. 9110–9138, 2021, doi: 10.1007/s10668-020-01015-2.
- [46] A. Diabat, D. Kannan, M. Kaliyan, and D. Svetinovic, “An Optimization Model for Product Returns Using Genetic Algorithms and Artificial Immune System,” *Resour. Conserv. Recycl.*, vol. 74, pp. 156–169, 2013, doi: 10.1016/j.resconrec.2012.12.010.
- [47] D. W. Clarke, “Adaptive Control,” *Ind Digit. Control Syst*, vol. 48, no. 5, pp. 190–220, 1986, doi: 10.31399/asm.hb.v16.a0002175.
- [48] Y. A. Mindzie, J. Kenfack, V. Joseph, U. Nzotcha, D. M. Djanssou, and R. Mbougouen, “Dynamic Performance Improvement using Model Reference Adaptive Control of Photovoltaic Systems Under Fast-Changing Atmospheric Conditions,” *Int. J. Photoenergy*, vol. 2023, 2023, doi: 10.1155/2023/5703727.
- [49] S. A. Frank, “Adaptive Control,” *SpringerBriefs Appl. Sci. Technol.*, pp. 85–89, 2018, doi: 10.1007/978-3-319-91707-8_11.
- [50] A. O. Ignat’ev, “On The Existence of Lyapunov Functions In Problems of Stability of Integral Sets,” *Ukr. Math. J.*, vol. 45, no. 7, pp. 1031–1041, 1993, doi: 10.1007/BF01057450.